PECULIARITIES OF THE DYNAMICS OF THE TOTAL ELECTRIC CURRENT AND ITS COMPONENTS IN ACTIVE REGIONS WITH DIFFERENT LEVELS OF FLASH PRODUCTIVITY

© 2025 Yu. A. Fursyak (https://orcid.org/0000-0001-8500-3478)

Crimean Astrophysical Observatory RAS, Nauchny, Republic of Crimea, Russia.

e-mail: yuriy_fursyak@mail.ru

Received February 22, 2025

Revised April 30, 2025

Accepted June 17, 2025

Abstract. The objective of the study is to analyze the dynamics of the total electric current and its components - vertical and horizontal electric currents - in active regions (ARs) with different levels of flash production. To calculate the value of the electric current, we used data from the Helioseismic and Magnetic Imager (HMI/SDO) instrument on the spatial distribution of the magnetic field vector components at the level of the Sun's photosphere. Seventy-three AOs of the 24th solar activity cycle were studied. Each region was monitored within ±35° relative to the central solar meridian, which corresponds to a time interval of 3-5 days. A number of peculiarities of the behavior of electric currents in AO were revealed. In particular, it is shown that: 1) Absolute values of the total electric current density in most of the considered cases are determined by the horizontal electric current, the density of which is 1.5-4.5 times greater than the vertical current density. 2) In 9 AOs (12% of the analyzed sample) the time intervals during which the mean unsigned density of the vertical electric current is approximately equal or exceeds the values of the mean unsigned density of the horizontal electric current were revealed. 3) In AOs NOAA 11158 and 12673, in which additional magnetic flux popping was recorded during the monitoring period, an increase in the vertical, horizontal, and total electric current was recorded 18-20 hours before the first flashes of high X-ray classes; the time interval of the increase in electric current parameters is significantly shorter than the time interval of the increase in the total unsigned magnetic flux of the AO. 4) The highest absolute values of the total electric current density were recorded in ARs with medium flare productivity.

DOI: 10.31857/S00167940250724e2

1. INTRODUCTION

Electric currents play an important role in the evolution of the active region (AR) and processes in the solar atmosphere. Already in 1967 it was noted that "the description of a number of processes in the solar atmosphere in terms of electric currents is often more interesting than in

magnetic field terms" [Alfven, Carlquist, 1967]. In recent decades, a number of important results related to the evolution and dynamics of the electric current at different heights in the Sun's atmosphere have been obtained. In particular, we would like to pay attention to the works of 2024 (e.g., [Bakunina et al., 2024; Melnikov, Meshalkina, 2024; Solov'ev 2024; Solov'ev, 2024; Solov'ev, Kirichek, 2024]).

The total electric current has two components - vertical and horizontal. The vertical electric current is easier to calculate - it requires data on the transverse magnetic field at a given level of the Sun's atmosphere. There are two approaches to calculating the vertical current - differential and integral. The differential method of calculating the vertical electric current can be called classical, since it was used already in the first works devoted to the study of electric currents in the Sun's atmosphere (see, e.g., Severnyi, 1965). The integral method began to be used only in the late 1980s of the 20th century [Abramenko and Gopasiuk, 1987], although the theoretical possibility of its application was considered as early as 1970 [Raylore and Semel, 1970].

The situation with the calculation of the horizontal electric current is much worse, because in this case, information on the vertical component of the magnetic field at least at two levels in the Sun's atmosphere is required. Although a number of two-channel magnetographs were created back in the 50s-60s of the 20th century [Stepanov and Severny, 1962; Severny, 1966; Ioshpa and Mogilevsky, 1965; Kuznetsov et al., 1966; Livingston, 1968, etc.], they have not been widely used until today. Moreover, systematic measurements of magnetic fields at two altitudes with good temporal and spatial resolution are absent even today. This makes it impossible to calculate the horizontal electric current directly from observations in two spectral lines formed at different heights, as was done in the 1960s-70s of the 20th century (see, e.g., [Kotov, 1970; Kotov, 1971]. Therefore, it is required to search for other ways of calculating the horizontal current, often indirect. And such methods were created. Thus, Hofmann and Staude estimated the azimuthal component of the electric current assuming a certain geometry of a strongly tilted magnetic tube forming an isolated sunspot [Hofmann and Staude, 1987]. Pevtsov and Peregud in 1990 assumed azimuthal (cylindrical) symmetry to obtain three components of the electric current [Pevtsov and Peregud, 1990]. In the late 1990s of the 20th century, Chinese astronomers proposed a rather interesting method for estimating horizontal electric currents. Their approach uses real vector magnetograms at one level of the solar atmosphere, which simultaneously serve as boundary conditions for calculating the magnetic field vector components at the second level [Ji et al., 1998]. In 2008, V.I. Abramenko also proposed an interesting method for calculating the horizontal current: considering a layer of small thickness, by simple mathematical calculations and some assumptions, it is possible to obtain an estimate of horizontal currents in the Sun's photosphere using data on the distribution of the vertical component of the magnetic field at only one level [Abramenko, 2008]. In 2017, this

method was finalized and tested [Fursyak, Abramenko, 2017]. It is this approach that is applied here to calculate the horizontal electric current. It should be noted that the absolute values of the horizontal electric current density obtained using the above methods agree well with each other and with the results of earlier works on the subject (e.g., [Kotov, 1970]).

The purpose of this work is to confirm, supplement, or correct, using more extensive statistical material, the results obtained earlier [Fursiak, 2024] on the study of the peculiarities of the dynamics of the total electric current and its components - vertical and horizontal currents - in ARs with different levels of flash productivity.

2. INITIAL DATA FOR ANALYSIS AND OBJECTS OF OBSERVATIONS

The input data for calculating the analyzed parameters of the magnetic field and electric currents are magnetographic data from the Helioseismic and Magnetic Imager (HMI, [Scherrer et al., 2012]) instrument on board the Solar Dynamics Observatory (SDO, [Pesnell et al., 2012]). We used SHARP (Space-Weather HMI Active Region Patches, [Bobra et al., 2014] magnetograms of the magnetic field vector components at the level of the Sun's photosphere in cylindrical coordinates with a temporal resolution of 12 min and a spatial resolution of 0.5″ pixel^{-1}(data series hmi.sharp_cea_720s), available at the Joint Science Operations Center (JSOC) website http://jsoc2.stanford.edu/ajax/lookdata.html. Together with the magnetographic data, we additionally downloaded from the JSOC website bitmap masks (which allow us to select the active region with a unique NOAA (National Oceanic and Atmospheric Administration) identifier on the rectangular SHARP magnetogram) and conf_disambig (which selects pixels on the magnetogram in which the uncertainty in the azimuth of the transverse magnetic field is resolved with a high degree of confidence, which is important for calculating the vertical electric current).

To plot the X-ray flux variations in the wavelength range of 1-8 Å in Earth orbit, we additionally used data from the GOES-15 spacecraft, available at https://www.ncei.noaa.gov/data/goes-space- environment-monitor/access/full/, as well as data from the catalog of the magneto-morphological classification (MMC) of ARs [Zhukova, 2018; Abramenko et al., 2018], developed at the Crimean Astrophysical Observatory (KRAO RAS) and modified in 2021 [Abramenko, 2021]. In addition to information on the type of ARs, the catalog also contains data on the most powerful flares recorded in the region and its flare index. The MMK AO catalog is available on the website of the Department of Solar and Solar System Physics of KRAO RAS at https://sun.crao.ru/databases/catalog-mmc-ars.

In this work, 73 AOs of the 24th solar activity cycle were studied. The main parameters of the investigated regions are presented in Table 1. The second column of the table contains the NOAA identifier of the region, and the third column contains the time of AO monitoring (corresponding to the time interval of 3-5 days, during which the region was within ±35° relative to the central solar

meridian). The fourth column shows the averaged value of the total unsigned magnetic flux for the AO monitoring time (averaging over time is indicated here by the line above). The total unsigned magnetic flux of AO was calculated according to the formula: $\Phi = s_{pix} \times \sum |B_z|_{bitmap+57s}$, where: s_{pix} - pixel area on the HMI/SDO magnetogram; $\sum |B_z|_{bitmap+57s}$ is the sum of absolute values of magnetic field strengths at >575 Gs (see Norton et al., 2017) inside the bitmap mask. The fifth column of the table indicates the type of the MMC region: U - unipolar; A - regions obeying the main empirical regularities established for sunspot groups (Hale's law of polarities, Joy's law, the rule of dominance of the area of the leading spot over the area of the main tail spot); B - regions violating the main empirical regularities established for sunspot groups. In the analyzed sample, there are 3 U-type, 28 A-type, and 42 B-type regions. The sixth column of the table contains information about the X-ray class of the most powerful flare recorded in the analyzed AO during its location on the visible disk of the Sun, and the date on which it was recorded. It is by the X-ray class of the most powerful flare that the flare productivity of the region is determined here. Accordingly, if only flares of X-ray class C are recorded in the AO, the flare productivity is considered low; if, in addition to flares of class C, flare events of X-ray classes M1.0 through M9.9 are also recorded, the flare productivity of the AO is considered medium; if at least one flare of X-ray class X1.0 and higher was recorded during the time the AO was located on the visible disk of the Sun, the flare productivity of the region is considered high. In the analyzed sample, regions with low flare productivity are 20, regions with medium flare productivity are 37, and regions with high flare productivity are 16. The seventh column indicates the value of the flash index (FI) of AO [Abramenko, 2005]: $FI = \frac{1}{\tau}\left(\sum C + 10\sum M + 100\sum X\right)$, where: τ - is the time (in days) of the AO on the visible disk of the Sun; $\sum C$, $\sum M$, $\sum X$ is, respectively, the total score of flares of X-ray classes C, M, and X recorded in the AO. According to the above formula, the flare index of AO will be equal to 1.0 (100.0), if one flare of X-ray class C1.0 (X1.0) is recorded in it every day. It follows from the data in Table 1 that the flare index of regions with low flare production does not exceed a few units, regions with medium production reach values from a few units to 20-30, AO with high flare production - is equal to several tens of units, and in some cases (in the presented sample these are the regions NOAA 12192 and 12673) - exceed a hundred units. Columns 8-10 of the table contain information on the average unsigned values of vertical, horizontal, and total electric current density in the AO, respectively, averaged over the monitoring period of the region. The data quadrature is

12 minutes. Taking into account the time of AO monitoring (3-5 days), averaging of electric current parameters is performed for 350-600 points. More details about the parameters presented in columns 8-10 of Table 1 are described below in Sections 3 and 4.

Table 1.

3. METHODS OF CALCULATION OF ANALYZED PARAMETERS

As already mentioned, to calculate the value of the total electric current, it is necessary to know the values of its components - vertical and horizontal electric currents.

To calculate the vertical electric current, the integral method is used here (Fursyak, 2018). It is based on the integral form of Ampere's law:

$$(j_z)_{i,j} = \frac{1}{\mu_0}\int_L B_t dl \qquad (1)$$

where: $\mu_0 = 4\pi \times 10^{-7}$ Gn m^{-1} is the magnetic constant; $\boldsymbol{B_t} \equiv (\boldsymbol{B_x}, \boldsymbol{B_y})$ is the AO transverse magnetic field vector; dl is the integration element equal to the pixel size on the HMI/SDO magnetogram (~363 km at the level of the Sun's photosphere at the center of the disk); i, j are the coordinates of the pixel on the magnetogram where the value of the vertical electric current is calculated. The integral in the right part of expression (1) is calculated approximated by Simpson's method. The integration contour$L$ has a rectangular shape and dimensions of 5×5 pixels. Averaging the current over the contour area$L$ gives the value of the vertical current density in its central pixel $(j_z)_{i,j}$.

The horizontal electric current is calculated using the methodology described in Fursyak, Abramenko [2017]. The initial formula is Ampere's law in differential form:

$$\mu_0 \boldsymbol{j} = \nabla \times \boldsymbol{B} \ , \qquad (2)$$

and the final formula for estimating the square of the horizontal current density is:

$$j_{\square}^2 = \frac{1}{\mu_0^2}\left[\left(\frac{\partial B_z}{\partial x}\right)^2 + \left(\frac{\partial B_z}{\partial y}\right)^2\right] \qquad (3)$$

As can be seen, expression 3 makes it possible to determine only the absolute value of the horizontal electric current density vector, but not its direction. Accordingly, it is also impossible to determine the direction of the total current vector. However, it is possible to calculate the absolute values of the total electric current density, knowing the values of the vertical and horizontal current density in each pixel of the original magnetogram:

$$|j| = \sqrt{(j_z)^2 + (j_{\square})^2} \ . \qquad (4)$$

Examples of distribution maps of absolute values of horizontal, vertical and total electric current density, as well as the map of the difference of absolute values of total and horizontal current density are presented in Fig. 1.

The values of the average unsigned densities of the vertical, horizontal and total electric current densities calculated inside the bitmap and conf_disambig masks were chosen as parameters characterizing the dynamics of the electric current in AO:

$$< |j_z| >= \frac{\Sigma |j_z|_{i,j}}{N}, \qquad < |j_h| >= \frac{\Sigma \sqrt{\left(j_{hx}^2\right)}_{i,j}}{N}, \qquad < |J| >= \frac{\Sigma J_{i,j}}{N} \quad , \tag{5}$$

where N is the number of pixels inside bitmap and conf_disambig masks.

It should be noted that the calculation errors of the electric current parameters are small. For the regions of the analyzed sample, the average values of unsigned densities of vertical, horizontal and total electric currents are at the level of 2σ-6σ.

Fig. 1.

4. RESULTS

Based on the obtained distribution maps of vertical, horizontal and total electric current densities, using expressions (5), the values of the average unsigned vertical $< |j_z| >$, horizontal $< |j_h| >$ and total $< |J| >$ electric current densities were calculated for the regions of the analyzed sample and plots of temporal variations of these parameters for each AO for the time interval of its monitoring were constructed. Examples of graphs of electric current parameters dynamics are shown in Fig. 2. Typical cases are presented.

Fig. 2.

As can be seen from the plots of Fig. 2, the average unsigned vertical electric current density $< |j_z| >$ differs for regions with different levels of flash productivity: higher values of this parameter are characteristic of ARs with higher flash productivity. At the same time, a similar pattern for the average unsigned horizontal and total electric current density is not observed. This suggests that the vertical electric current is associated with flashiness in ARs, while the horizontal current is involved in other processes.

Also from the graphs presented in Figure 2, as well as the data in Table 1 (columns 8-9), we can see that in most of the considered cases the average unsigned horizontal electric current density is 1.5-4.5 times larger than the corresponding values of the average unsigned vertical current density. The main contribution to the absolute values of the magnitude of the total electric current is thus given by the horizontal current. However, for 9 AOs, which is 12% of the areas of the analyzed sample, there are time intervals within which the value of the average unsigned vertical electric current density is approximately equal to or exceeds the value of the average unsigned horizontal current density (examples are presented in Fig. 3) during a significant time interval. Table 2 summarizes the areas where this effect has been recorded and the time (in

hours) over which the value of $\langle |j_z| \rangle$ is approximately equal to or greater than the value of $\langle |j_h| \rangle$. Possible reasons for this feature of the dynamics of electric current parameters should be considered separately.

Fig. 3.

Table 2.

It is extremely interesting to analyze the dynamics of the electric current parameters in the NOAA 11158 and 12673 regions, in which additional magnetic flux resurfacing was observed during the monitoring period, due to which the total magnetic flux of the AO changed by more than an order of magnitude (Fig. 4). First of all, one can note rather strong fluctuations of the horizontal and total electric current density values even before the beginning of the magnetic flux resurfacing. In the NOAA 11158 region, these oscillations are recorded 16 hours before the magnetic flux resurfacing, in the NOAA 12673 region - approximately two hours. At the same time, no significant changes in the value of the mean unsigned vertical electric current density are not observed at this time. A rather rapid increase of $\langle |j_z| \rangle$ above the threshold value of 2.7 mA $m^{(-2)}$ (this value is described in more detail in Fursyak et al., 2020) begins in the NOAA 11158 region 6 hours after the onset of magnetic flux resurfacing, in the NOAA 12673 region - 17 hours, and in both cases lasts for about 6 hours (this time interval is marked by vertical dashed lines in the plots of Fig. 4). This observation indicates redistributions of magnetic energy in the AO. It should be noted that the redistribution (growth) of magnetic energy associated with the evolution of the vertical electric current is directly shown in (Nechaeva et al., 2024). Almost simultaneously (a lag of no more than one and a half hours), the increase of the parameters $\langle |j_h| \rangle$ and $\langle |J| \rangle$ also begins, but here the time of increase of the corresponding values is longer (about 10 hours in the NOAA 11158 region and more than a day in the NOAA 12673 region). These results also indicate that the components of the total electric current - horizontal and vertical currents - are associated with different processes in the Sun's atmosphere. The dynamics of electric currents, magnetic flux, magnetic energy, and other parameters for AOs NOAA 11158 and 12673 have also been investigated in several other works (e.g., [Sun et al., 2012; Wang et al., 2018]. It should also be noted that the increase in the analyzed electric current parameters is recorded 18-20 h before the first flashes of high X-ray classes. At the same time, the growth of the total unsigned AO magnetic flux is observed on a significantly longer time scale (tens of hours) than the growth of the electric current parameters.

Fig. 4.

On the basis of the data presented in columns 7-10 of Table 1, we plot the dependence of the AO flash index on the values of the analyzed electric current parameters averaged over the time of monitoring the region (Fig. 5). The left panels of Fig. 5 additionally color-code the AO flare

productivity (see the sixth column of Table 1), while the right panels show the type of region according to the MMC (see the fifth column of Table 1).

Fig. 5.

As follows from the plots of Fig. 5, some kind of dependence can be traced only for the pair $< |\overline{j_z}| > -FI$, which confirms the above assumption that vertical electric currents are more closely related to flashes in AO than horizontal currents. Here we can also highlight the boundary values of the parameter $< |j_z| >$ (vertical dashed lines in panel (a) of Fig. 5): 2.85 mA m^{-2}, which marks the minimum value of $< |\overline{j_z}| >$ for ARs with high flash production (at the same time, this value is the lower limit of $< |j_z| >$ for regions of group B3 according to the IMC (panel (b) of Fig. 5)), and 3.3 mA m^{-2}, which marks the maximum value of $< |j_z| >$ for ARs with low flash production. Within the indicated limits of the values of the mean unsigned vertical electric current density, the flare productivity of ARs is probably determined by additional factors and parameters, e.g., the motions of individual spots in the group, the compactness of ARs, the surfacing of new, even relatively small, magnetic fluxes, etc. Further investigation of the regions falling within this range of values of the magnitude $< |j_z| >$ is required.

Further, the values of the flash index and electric current parameters were averaged, respectively, over the set of ARs of the analyzed sample with low (n = 20), medium (n = 37), and high (n = 16) flash productivity. The results of the averaging are presented in Table 3 and the dependency plots are presented in Figure 6. The following can be seen:

- We can see (see panel (a) of Fig. 6) a stepwise relationship between the averaged value of the average unsigned vertical electric current density $mean(< |j_z| >)$ and the averaged flash index ($mean(FI)$).

- The dependence between the averaged value of the average unsigned horizontal electric current density $mean\left(< \left|\overrightarrow{j_{\square}}\right| >\right)$ and the averaged flash index ($mean(FI)$), as well as the dependence $mean(< |j| >) - mean(FI)$ is more complex (see panels (b) and (c) of Fig. 6). It can be seen that the value of the parameters $mean\left(< \left|\overrightarrow{j_{\square}}\right| >\right)$ and $mean(< |j| >)$ are larger for ARs with average flashiness than for regions with high flashiness. Thus, the earlier assumption [Fursiak, 2024] that this effect is due to a selection effect turned out to be incorrect: ARs with medium flash production do indeed have statistically higher values of the mean unsigned horizontal electric current density than regions with high and low flash production. Attempting to explain this observation will be the goal of further research.

Table 3.

Fig. 6.

5. CONCLUSIONS AND DISCUSSION

The study of the dynamics of vertical, horizontal and total electric current carried out on a sample of 73 AOs allowed us to clarify the results obtained earlier (Fursiak, 2024). Based on the analyzed material, the following conclusions can be drawn:

1. In most of the cases considered, the value of the average unsigned horizontal electric current density is 1.5-4.5 times greater than the value of the vertical current density. The absolute value of the total electric current is thus determined predominantly by the horizontal current.

2. In 9 AOs, which is more than 12% of the analyzed sample, time intervals with duration from 6 to 64 hours, within which the value of the average unsigned vertical electric current density is approximately equal to or greater than the average unsigned horizontal current density, were detected.

3. In the NOAA 11158 and 12673 regions, in which the surfacing of new magnetic fluxes was recorded during the period of their monitoring, there is an increase in the mean unsigned magnitudes of the vertical, horizontal, and total electric current 18-20 hours before the first flashes of high X-ray classes; the time interval of the increase in the electric current parameters (from several hours to several tens of hours) is much shorter than the time interval of the increase in the magnitude of the total unsigned magnetic flux. This result agrees well with the results of several other studies (e.g., [Nechaeva et al., 2024]).

4. A step dependence between the average unsigned vertical electric current density and the AO flash index was found; there is no dependence between the magnitude of the total electric current and the AO flash productivity.

5. The highest absolute values of the horizontal and total electric current density values were recorded in the regions with average flash productivity.

A number of peculiarities of the dynamics of electric current parameters revealed in this work require additional studies:

- oscillations of the values of the mean unsigned densities of horizontal and total electric currents before the surfacing of new magnetic fluxes detected in NOAA regions 11158 and 12673; if this feature is confirmed on a larger statistical material, we can talk about the detection of a predictor of the surfacing of a new magnetic flux in AR;

- existing differences in the level of AO flare productivity with simultaneous equality of the values of the mean unsigned vertical electric current densities; it is required to search for additional criteria, effects or features of the AO evolution, which can additionally influence the activity of the region;

- statistically detected excess of values of mean unsigned horizontal electric current densities in ARs with medium flash productivity compared to areas with low and high flash productivity; and

others.

FUNDING

This work was supported by the Ministry of Education and Science of the Russian Federation, GZ #122022400224-7.

CONFLICT OF INTERESTS

The author of this paper declares no conflict of interest.

REFERENCES

1. *Abramenko V.I., Gopasyuk S.I.* The system of electric currents and the structure of the magnetic field of the active region // Izv. Krymsk. Astrophysics. V. 76. P. 147-168. 1987.
2. *Zhukova A.V.* Catalog of active regions of the 24th cycle // Izv. Krymsk. Astrophysics. V. 114. No. 2. P. 74-86. 2018.
3. *Ioshpa B.A., Mogilevsky E.I.* IZMIRAN magnetograph for determining the longitudinal component of the magnetic fields of active regions // Solar activity. No. 2. 1965.
4. *Kotov V.A.* Magnetic field and electric currents of a unipolar sunspot // Izv. Krymsk. Astrophysics. obs. V. 41-42. P. 67-88. 1970.
5. *Kuznetsov D.A., Kuklin G.V., Stepanov V.E.* Solar magnetograph and radial velocity recorder // The results of observations and research during the MGSS period. No. 1. 1966.
6. *Severny A.B.* On magnetic fields at different depths of the solar atmosphere // Astronomical Journal. V. 43. No. 3. P. 465-479. 1966.
7. *Stepanov V.E., Severny A.B.* Photoelectric method for measuring the magnitude and direction of the magnetic field on the surface The Sun // Izv. Krymsk. Astrophysics. obs. V. 28. P. 166-193. 1962.
8. *Fursyak Yu.A.* Full electric current in active areas with different levels of flash productivity: the first results // Izv. Krymsk. Astrophysics. Observ. V. 120. No. 4. P. 46-55. 2024.
9. *Abramenko V.I.* Relationship between magnetic power spectrum and flare productivity in solar active regions // Astrophys. J. V. 629. No. 2. P. 1141-1149. 2005.
10. *Abramenko V.I.* Spectrum of Magnetic Dissipation and Horizontal Electric Currents in the Solar Photosphere // eprint arXiv:0806.1547. 2008.
11. *Abramenko V.I.* Signature of the turbulent component of the solar dynamo on active region scales and its association with flaring activity // Monthly Notices of the Royal Astronomical Society. Vol. 507. Issue 3. P. 3698-3706. 2021.
12. *Abramenko V.I., Zhukova A.V., Kutsenko A.S.* Contributions from different-type active regions into the total solar unsigned magnetic flux // Geomagnetism and Aeronomy. Vol. 58. Issue 8. P. 1159-1169. 2018.

13. *Alfven H., Carlquist P.* Currents in the Solar Atmosphere and a Theory of Solar Flares // Solar Physics. Vol. 1. Issue 2. P. 220–228. 1967.
14. *Bakunina I.A., Melnikov V.F., Shain A.V., Kuznetsov S.A., Abramov-Maximov V.E.* Spatial Position of Magnetic Flux Ropes in Flare Active Regions with and without Coronal Mass Ejections // Geomagnetism and Aeronomy. Vol. 64. No. 8. P. 1237–1249. 2024.
15. *Bobra M.G., Sun X., Hoeksema J.T., et al.* The Helioseismic and Magnetic Imager (HMI) vector magnetic field pipeline: SHARPs – Space-Weather HMI Active Region Patches // Solar Phys. Vol. 289. Issue 9. P. 3549-3578. 2014.
16. *Fursyak Yu.A.* Vertical Electric Currents in Active Regions: Calculation Methods and Relation to the Flare Index // Geomagnetism and Aeronomy. Vol. 58. Issue 8. P. 1129–1135. 2018.
17. *Fursyak Yu.A., Abramenko V.I.* Possibilities for Estimating Horizontal Electrical Currents in Active Regions on the Sun // Astrophysics. Vol. 60. Issue 4. P. 544-552. 2017.
18. *Fursyak Yu.A., Abramenko V.I., Kutsenko A.S.* Dynamics of Electric Current's Parameters in Active Regions on the Sun and Their Relation to the Flare Index // Astrophysics. Vol. 63. Issue 2. P. 260-273. 2020.
19. *Hofmann A., Staude J.* Electric current density in the sunspot photosphere derived from vector magnetograms // Publications of the Astronomical Institute of the Czechoslovak Academy of Sciences. Vol. 66. P. 105-107. 1987.
20. *Ji H.S., Song M.T., Li X.Q., Hu F.M.* Estimating Horizontal Electric Current in Solar Active Regions // Solar Physics. Vol. 182. Issue 2. P. 365–379. 1998.
21. *Kotov V.A.* On the Structure of Magnetic Field and Electric Currents of a Unipolar Sunspot // Solar Magnetic Fields. IAU Symposium. Vol. 43. P. 212-219. 1971.
22. *Livingston W.C.* Magnetograph Observations of the Quiet Sun. I. Spatial Description of the Background Fields // Astrophysical Journal. Vol. 153. P. 929-942. 1968.
23. *Melnikov V.F., Meshalkina N.S.* Contraction Effect of Coronal Loops during the Flare of February 24, 2023 // Geomagnetism and Aeronomy. Vol. 64. No. 8. P. 1381–1385. 2024.
24. *Nechaeva A.B., Zimovets I.V., Zubik V.S., Sharykin I.N.* Evolution of Characteristics of Vertical Electric Current and Magnetic Field in Active Regions of the Sun and Their Relation to Powerful Flares // Geomagnetism and Aeronomy. Vol. 64. No. 2. P. 150–171. 2024.
25. *Pesnell W.D., Thompson B.J., Chamberlin P.C.* The Solar Dynamics Observatory (SDO) // Solar Phys. Vol. 275. Issue 1-2. P. 3-15. 2012.
26. *Scherrer P.H., Schou J., Bush R.I., et al.* The Helioseismic and Magnetic Imager (HMI) investigation for the Solar Dynamics Observatory (SDO) // Solar Phys. Vol. 275. Issue 1-2.

P. 207-227. 2012.

27. *Severnyi A.B.* The Nature of Solar Magnetic Fields (The Fine Structure of the Field) // Soviet Astronomy. Vol. 9. No. 2. P. 171-182. 1965.
28. *Solov'ev A.A.* Flare filament with the force free structure of the magnetic field // Geomagnetism and Aeronomy. Vol. 64. No. 7. P. 188-194. 2024.
29. *Solov'ev A.A.* Force free magnetic flux rope with high electric current density on the axis // Astronomical Reports. Vol. 68. No. 6. P. 601-609. 2024.
30. *Solov'ev A.A., Kirichek E.A.* Magnetic Flux Ropes with a Current Shell As Flaring Solar Structures // Astronomy Letters. Vol. 50. No. 9. P. 584–592. 2024.
31. *Sun X., Hoeksema J.T, Liu Y., Wiegelmann T., Hayashi K, Chen Q., Thalmann J.* Evolution of Magnetic Field and Energy in a Major Eruptive Active Region Based on SDO/HMI Observation // Astrophysical Journal. Vol. 748. Article id. 77. 2012.
32. *Rayrole J., Semel M.* Evaluation of the electric current in a sunspot by the study of the observed transverse component of the magnetic field // Astron. Astrophys. Vol. 6. P. 288-293. 1970.
33. *Wang R., Liu Y.D., Hoeksema J.T., Zimovets I.V., Liu Y.* Roles of Photospheric Motions and Flux Emergence in the Major Solar Eruption on 2017 September 6 // Astrophysical Journal. Vol. 869. Article id. 90. 2018.

Table 1. Parameters of analyzed AOs

№ n/a	Area number (NOAA)	AO monitoring time	—	Type of AO according to IMC	Maximum flash	FI	$\langle \overline{\lvert B_z \rvert} \rangle$, mA m^{-2}	$\langle \overline{\lvert j_\square \rvert} \rangle$, mA m^{-2}	$\langle \overline{\lvert B \rvert} \rangle$, mA m^{-2}
1	2	3	4	5	6	7	8	9	10
1	11158	12.02.-15.02.2011	0.75	B2	X2.2, 15.02.2011	59.26	4.10	7.07	8.18
2	11261	31.07.-03.08.2011	0.96	B3	M9.3, 04.08.2011	28.68	4.21	10.10	10.96
3	11263	02.08.-05.08.2011	0.89	B2	X6.9, 09.08.2011	63.47	3.51	4.18	5.47
4	11283	04.09.-07.09.2011	0.39	B2	X2.1, 06.09.2011	45.61	3.12	3.99	5.10
5	11302	27.09.-30.09.2011	1.49	A2	X1.9, 24.09.2011	78.79	3.53	6.57	7.47
6	11305	29.09.-02.10.2011	0.54	A1	M3.9, 02.10.2011	6.37	3.28	6.21	7.07
7	11339	06.11.-10.11.2011	2.58	A2	X1.9, 03.11.2011	38.17	3.00	7.84	8.40
8	11391	07.01.-10.01.2012	0.95	A1	C2.2, 13.01.2012	0.30	2.76	9.34	9.74
9	11429	07.03.-10.03.2012	2.41	B2	X5.4, 07.03.2012	70.89	3.56	8.66	9.38
10	11476	09.05.-13.05.2012	2.40	B3	M5.7, 10.05.2012	30.55	3.98	9.35	10.17
11	11512	27.06.-30.06.2012	0.59	A1	C4.2, 28.06.2012	1.17	2.90	9.55	9.98
12	11520	10.07.-14.07.2012	4.62	B3	X1.4, 12.07.2012	13.38	2.85	7.32	7.86
13	11598	25.10.-29.10.2012	0.37	B1	M5.0, 22.10.2012	5.03	3.15	6.23	7.00
14	11618	20.11.-	0.48	B3	M1.6,	6.75	4.22	4.60	6.23

		23.11.2012			27.11.2012				
15	11654	12.01.-16.01.2013	2.36	B2	M1.0, 11.01.2013	3.26	3.06	7.57	8.16
16	11711	04.04.-07.04.2013	0.29	A1	C1.7, 03.04.2013	0.17	2.35	5.50	5.99
17	11748	18.05.-21.05.2013	0.32	B3	X1.2, 15.05.2013	15.98	3.40	7.28	8.04
18	11778	27.06.-30.06.2013	0.36	A1	M2.9, 23.06.2013	6.32	2.51	8.06	8.45
19	11861	11.10.-14.10.2013	0.30	B1	C8.5, 18.10.2013	6.89	3.20	3.75	4.95
20	11882	28.10.-01.11.2013	0.76	B1	M4.4, 28.10.2013	14.00	3.04	8.07	8.63
21	11890	07.11.-10.11.2013	1.48	A2	X3.3, 05.11.2013	55.63	3.23	9.89	10.40
22	11899	17.11.-20.11.2013	1.96	U2	M1.1, 23.11.2013	3.85	2.55	6.37	6.87
23	11936	27.12.-31.12.2013	0.45	B2	M9.9, 01.01.2014	18.50	3.18	3.85	5.02
24	11944	06.01.-09.01.2014	2.87	B2	X1.2, 07.01.2014	31.71	2.96	5.33	6.10
25	11946	06.01.-09.01.2014	0.92	B1	M1.0, 07.01.2014	1.62	3.09	11.23	11.65
26	11968	01.02.-05.02.2014	1.38	B2	M3.8, 04.02.2014	11.76	3.22	10.12	10.62
27	11974	10.02.-13.02.2014	1.34	B2	M3.7, 12.02.2014	22.66	4.14	10.46	11.26
28	11991	02.03.-05.03.2014	0.59	B2	M1.1, 28.02.2014	6.02	3.52	7.79	8.56
29	12002	12.03.-15.03.2014	0.80	A2	M1.7, 10.03.2014	9.58	3.01	7.71	8.30
30	12014	24.03.-27.03.2014	0.77	B1	M1.7, 20.03.2014	4.90	2.67	8.15	8.60
31	12017	25.03.-	0.52	A1	X1.0,	12.54	3.01	8.20	8.74

		29.03.2014			29.03.2014				
32	12109	07.07.-10.07.2014	1.35	B1	C6.5, 13.07.2014	2.55	3.15	9.12	9.65
33	12149	26.08.-29.08.2014	0.58	A2	M1.2, 22.08.2014	7.02	2.75	3.69	4.61
34	12152	31.08.-03.09.2014	0.71	A2	M2.5, 03.09.2014	4.47	2.84	6.76	7.34
35	12158	09.09.-12.09.2014	1.17	B1	X1.6, 10.09.2014	13.00	3.28	7.43	8.13
36	12192	22.10.-25.10.2014	8.37	B3	X3.1, 24.10.2014	101.64	3.20	11.93	12.35
37	12205	08.11.-12.11.2014	0.98	B2	X1.6, 07.11.2014	47.15	3.53	8.58	9.29
38	12222	30.11.-04.12.2014	1.90	A2	M1.8, 01.12.2014	10.65	2.87	10.02	10.43
39	12241	17.12.-21.12.2014	1.83	B3	M8.7, 17.12.2014	20.79	3.38	10.38	10.92
40	12253	03.01.-06.01.2015	1.74	A2	M1.3, 04.01.2015	7.83	2.91	11.50	11.87
41	12268	27.01.-30.01.2015	1.31	B2	M2.1, 29.01.2015	7.61	2.84	6.52	7.11
42	12277	01.02.-05.02.2015	1.49	B1	M1.7, 30.01.2015	7.04	2.60	7.17	7.64
43	12290	22.02.-26.02.2015	0.43	A1	M8.2, 03.03.2015	8.97	2.35	9.01	9.32
44	12297	11.03.-14.03.2015	0.83	B3	X2.2, 11.03.2015	46.32	4.62	4.40	6.43
45	12303	21.03.-24.03.2015	0.24	U2	C3.2, 29.03.2015	1.42	2.20	5.74	6.15
46	12305	25.03.-29.03.2015	1.08	B1	C8.7, 25.03.2015	1.33	2.69	4.84	5.57
47	12320	06.04.-09.04.2015	0.14	B2	M1.4, 08.04.2015	6.42	3.01	4.60	5.58
48	12335	05.05.-	0.86	B2	M2.6,	6.71	2.95	9.16	9.63

		08.05.2015			05.05.2015				
49	12339	10.05.- 13.05.2015	2.17	B2	M1.9, 06.05.2015	8.79	2.83	6.86	7.43
50	12365	09.06.- 13.06.2015	0.13	B1	C1.8, 10.06.2015	0.21	2.88	4.81	5.64
51	12367	15.06.- 19.06.2015	1.46	A2	M3.8, 21.06.2015	6.82	2.61	11.32	11.62
52	12371	20.06.- 23.06.2015	2.69	B1	M7.9, 25.06.2015	18.23	3.22	8.60	9.19
53	12381	07.07.- 10.07.2015	1.07	A1	M1.7, 06.07.2015	5.25	2.94	5.84	6.57
54	12396	06.08.- 09.08.2015	1.86	A2	C5.4, 07.08.2015	2.93	3.15	9.22	9.75
55	12403	22.08.- 25.08.2015	2.64	A2	M5.6, 24.08.2015	30.10	3.60	11.85	12.38
56	12421	23.09.- 27.09.2015	0.25	B1	C9.4, 27.09.2015	1.74	3.31	7.99	8.67
57	12443	02.11.- 05.11.2015	1.87	B2	M3.7, 04.11.2015	11.84	2.78	12.40	12.71
58	12470	17.12.- 21.12.2015	0.34	U1	C4.6, 18.12.2015	0.64	2.33	4.98	5.51
59	12473	25.12.- 30.12.2015	1.20	B2	M4.7, 23.12.2015	9.02	2.89	9.19	9.65
60	12480	10.01.- 14.01.2016	0.56	A1	C1.7, 15.01.2016	0.23	2.26	6.84	7.21
61	12492	05.02.- 09.02.2016	0.18	B1	C2.1, 12.02.2016	0.41	2.69	7.06	7.58
62	12494	05.02.- 07.02.2016	0.67	B1	C5.2, 04.02.2016	1.77	3.00	9.68	10.14
63	12506	26.02.- 01.03.2016	0.35	B1	C3.3, 27.02.2016	0.52	2.92	6.83	7.43
64	12521	13.03.- 16.03.2016	0.30	A1	C1.0, 15.03.2016	0.36	2.86	10.90	11.27
65	12529	12.04.-	2.74	A2	M6.7,	8.10	2.74	8.76	9.18

		16.04.2016			18.04.2016				
66	12546	18.05.-22.05.2016	0.81	A1	C1.3, 24.05.2016	0.57	2.60	5.77	6.35
67	12615	02.12.-05.12.2016	0.67	A1	M1.2, 30.11.2016	4.40	2.89	9.54	9.97
68	12644	27.03.-30.03.2017	0.04	A2	M5.8, 03.04.2017	19.27	2.88	3.09	4.28
69	12661	05.06.-09.06.2017	0.21	B1	C8.0, 02.06.2017	2.39	2.41	6.69	7.13
70	12665	10.07.-13.07.2017	1.86	A2	M2.4, 14.07.2017	6.53	2.93	10.94	11.33
71	12673	02.09.-05.09.2017	0.92	B3	X9.3, 06.09.2017	223.86	3.99	8.75	9.63
72	12674	03.09.-06.09.2017	1.40	A1	C5.2, 30.08.2017	0.76	2.49	4.76	5.38
73	12699	09.02.-12.02.2018	0.65	A1	C8.1, 07.02.2018	1.30	2.84	9.07	9.52

Table 2. Some AO parameters, in which the exceeding of the values of the average unsigned vertical electric current density over the values of the horizontal current was recorded during the monitoring period

excess of the values of the average unsigned vertical electric current density over the horizontal current values

No. n/a	Region number (NOAA)	T, h	Type of AO by MMK	FI	Outbreak productivity of AO
1	11263	34	B2	63.47	High
2	11283	34	B2	45.61	High
3	11618	39	B3	6.75	Medium
4	11861	47	B1	6.89	Low
5	11936	57	B2	18.50	Medium
6	12149	6	A2	7.02	Average
7	12297	64	B3	46.32	High
8	12320	32	B2	6.42	Medium
9	12644	57	A2	19.27	Average

Table 3. Averaged flashover indices and electric current parameters for the set of areas of the analyzed sample with low, medium and high flash productivity

	$mean(FI)$	$mean < \lvert j_z \rvert >$	$mean < \lvert j_{\square} \rvert >$	$mean < \lvert j \rvert >$
Areas with low flash production (n = 20)	1.38±0.72	2.75±0.16	7.12±0.98	7.68±0.93
Areas with medium flash productivity (n = 37)	10.69±2.64	3.07±0.16	8.19±0.84	8.82±0.77
Areas with high flash productivity (n = 16)	57.34±28.18	3.43±0.28	7.34±1.16	8.19±1.01

FIGURE CAPTIONS

Fig. 1. Distribution maps of absolute values of vertical (a), horizontal (b), and total (c) electric current densities, as well as a map of the difference between total and vertical electric current densities (d) at the time of 00:00UT on February 15, 2011 (approximately 3 hours before the first X-class X-ray flare in the 24th solar cycle). The maps are normalized: (a) -5 (black) to 15 (white) mA m^{-2}; (b) - -15 (black) to 45 (white) mA m^{-2}; (c) -15 (black) to 45 mA (white) m^{-2}; (d) - 2.5 (black) to 7.5 (white) mA m^{-2}. The contours indicate: gray bold - bitmap mask, gray thin - conf_disambig mask; thin black - main spots in AO with $|B_z| \geq 1000$ GS.

Fig. 2. Typical picture of the dynamics of the magnitudes of the mean unsigned vertical (black bold curve), horizontal (gray bold curve), and total (double curve) electric current densities in regions with low (a), medium (b), and high (c) flash production. Also shown are the dynamics of the total unsigned magnetic flux AO (thin black curve, scale on the right); the solar X-ray flux in the wavelength range 1-8Å at the Earth's orbit using data from the GOES-15 spacecraft (dashed curve). The horizontal dashed line with a long stroke shows the threshold level of the value of the mean unsigned vertical electric current density of 2.7 mA m^{-2} (see Fursyak et al., 2020, for more details). The plots indicate the X-ray classes of the most powerful flares recorded in the AO during its monitoring period. The bars of the largest errors in the calculation of the mean unsigned values of the electric currents are indicated.

Fig. 3. Examples of the dynamics of electric current parameters in the regions of the analyzed

sample, in which a time interval was found during the AO monitoring period, during which the value of the mean unsigned vertical electric current density is approximately equal to or exceeds the value of the mean unsigned horizontal current density (this interval is shaded gray in the graphs). Other notations are the same as in Fig. 2.

Fig. 4. Dynamics of electric current parameters in the regions NOAA 11158 and 12673 of the analyzed sample, in which a significant increase of the total unsigned magnetic flux was observed during their monitoring. The designations are the same as in Fig. 2. Additionally, we show: the time interval of rapid increase in the value of the average unsigned vertical electric current density (vertical dashed lines); the time interval of increase in the total unsigned magnetic flux AO (gray shaded area).

Fig. 5. Dependences of the AO flash index (FI) on the average unsigned vertical (a, b), horizontal (c, d), and total (e, f) electric current densities, respectively. The color of the symbols in the left panels (a, c, e) encodes the AO flash productivity, while the right panels indicate the type of AO according to the IMC. The legends are appended. Error bars and correlation coefficients between the corresponding pairs of values are indicated.

Fig. 6. Same as Fig. 5, but averaged over the population of AOs of the analyzed sample with low (light dots), medium (gray dots), and high (black dots) flash productivity. Circles of the corresponding color indicate data obtained in an earlier study (Fursiak, 2024) on a sample of 12 AOs. Error bars and correlation coefficients between corresponding pairs of values are indicated.

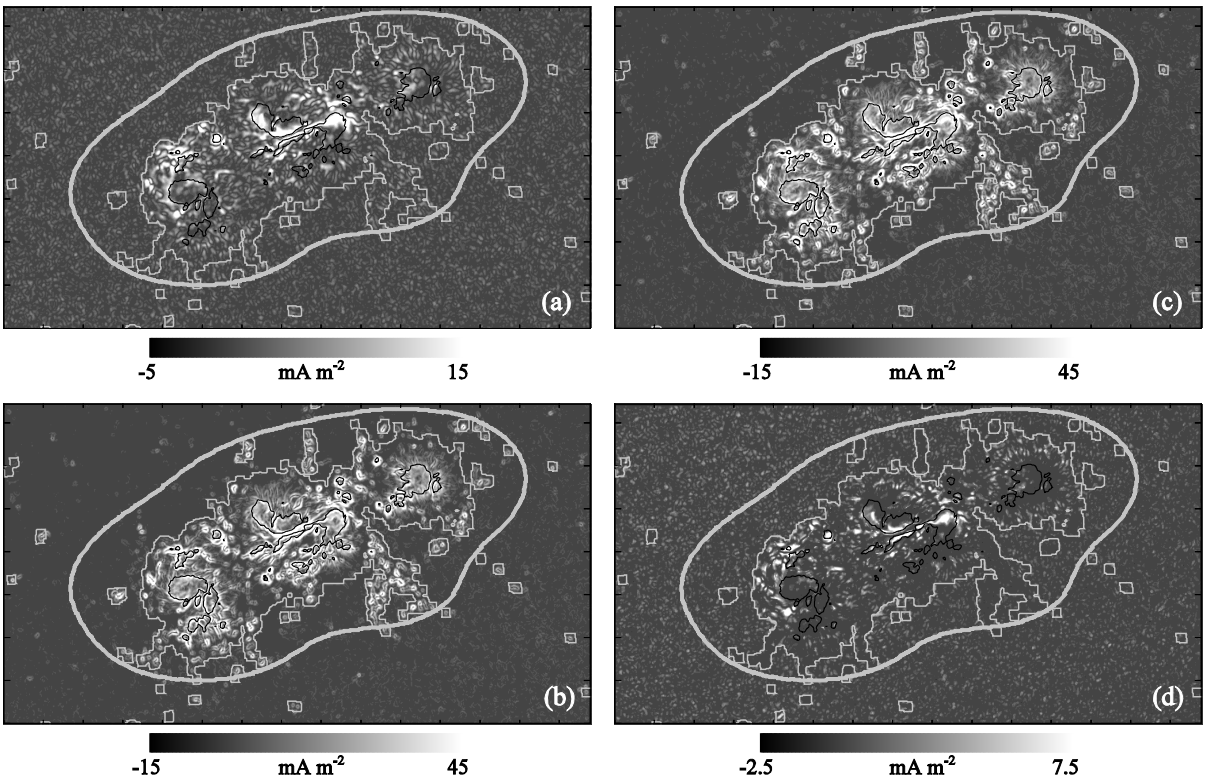

AR NOAA 11158 00:00UT 15.02.2011

Fig. 1.

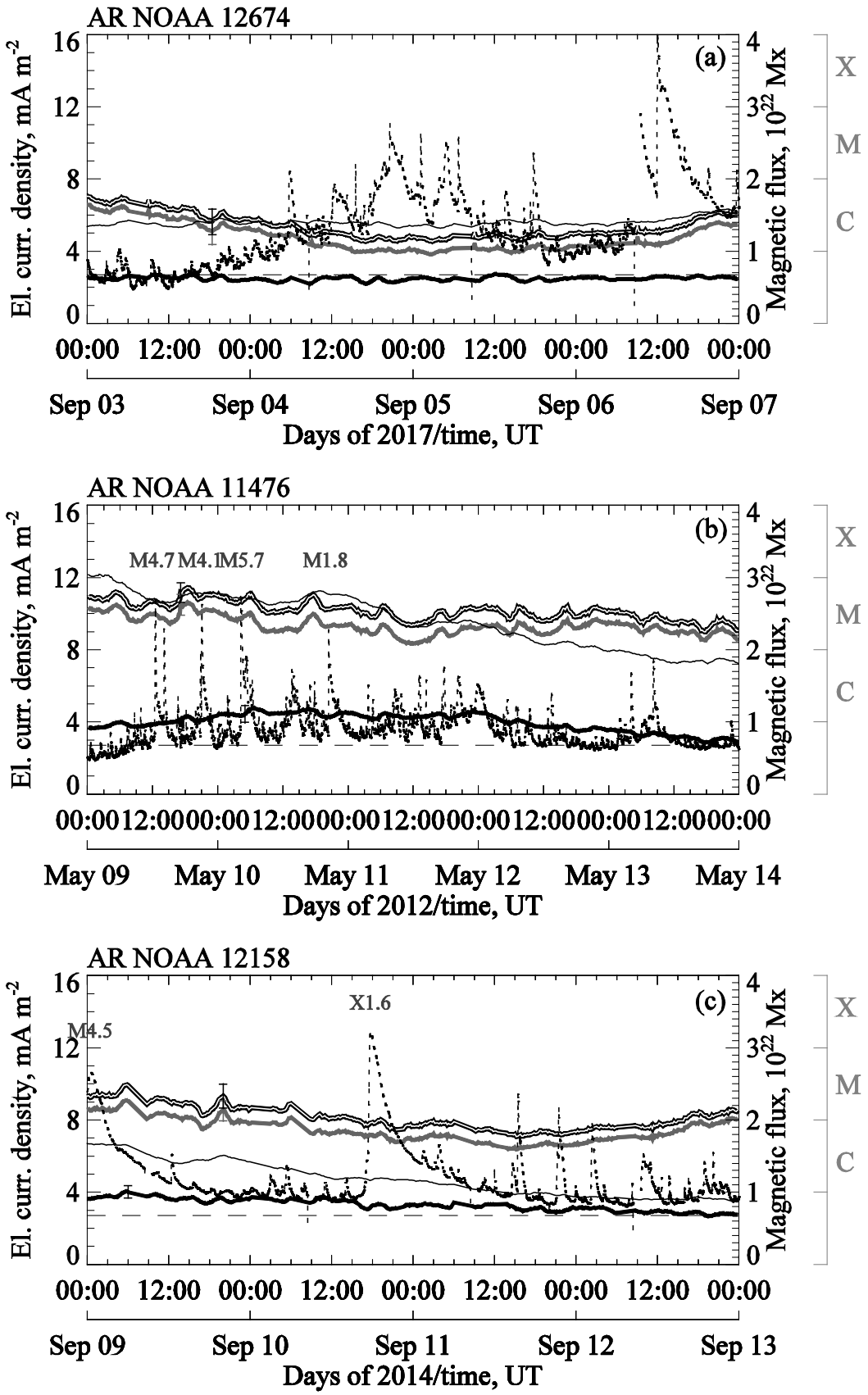
AR NOAA 12674
(a)
El. curr. density, mA m-2
Magnetic flux, 10^22 Mx
X
M
C
00:00 12:00 00:00 12:00 00:00 12:00 00:00 12:00 00:00
Sep 03 Sep 04 Sep 05 Sep 06 Sep 07
Days of 2017/time, UT
AR NOAA 11476
(b)
M4.7 M4.1 M5.7 M1.8
May 09 May 10 May 11 May 12 May 13 May 14
Days of 2012/time, UT
AR NOAA 12158
(c)
X1.6
M4.5
Sep 09 Sep 10 Sep 11 Sep 12 Sep 13
Days of 2014/time, UT

Fig. 2.

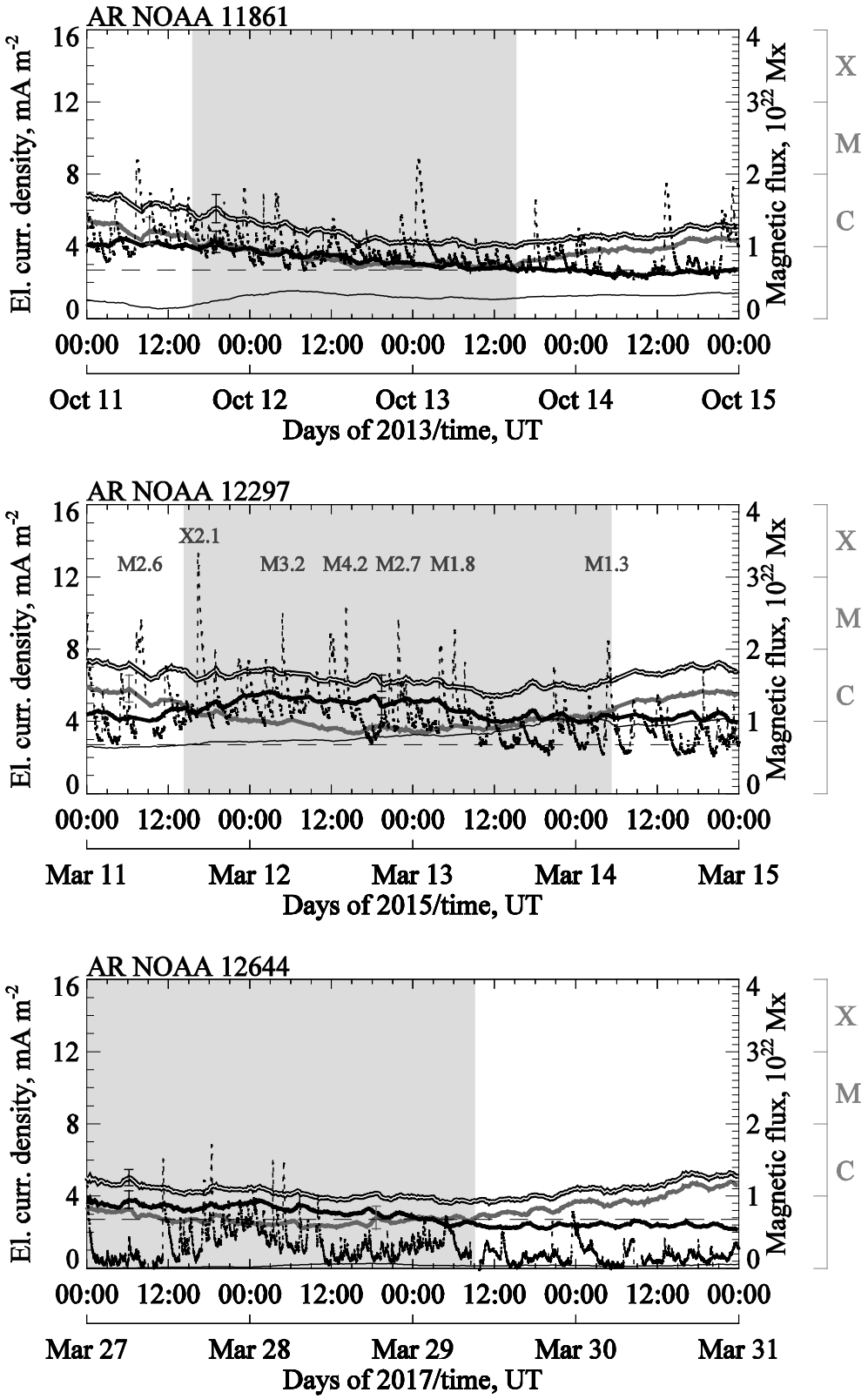
AR NOAA 11861
El. curr. density, mA m-2
Magnetic flux, 10^22 Mx
X
M
C
00:00 12:00 00:00 12:00 00:00 12:00 00:00 12:00 00:00
Oct 11
Oct 12
Oct 13
Oct 14
Oct 15
Days of 2013/time, UT
AR NOAA 12297
X2.1
M2.6
M3.2
M4.2
M2.7
M1.8
M1.3
Mar 11
Mar 12
Mar 13
Mar 14
Mar 15
Days of 2015/time, UT
AR NOAA 12644
Mar 27
Mar 28
Mar 29
Mar 30
Mar 31
Days of 2017/time, UT

Fig. 3.

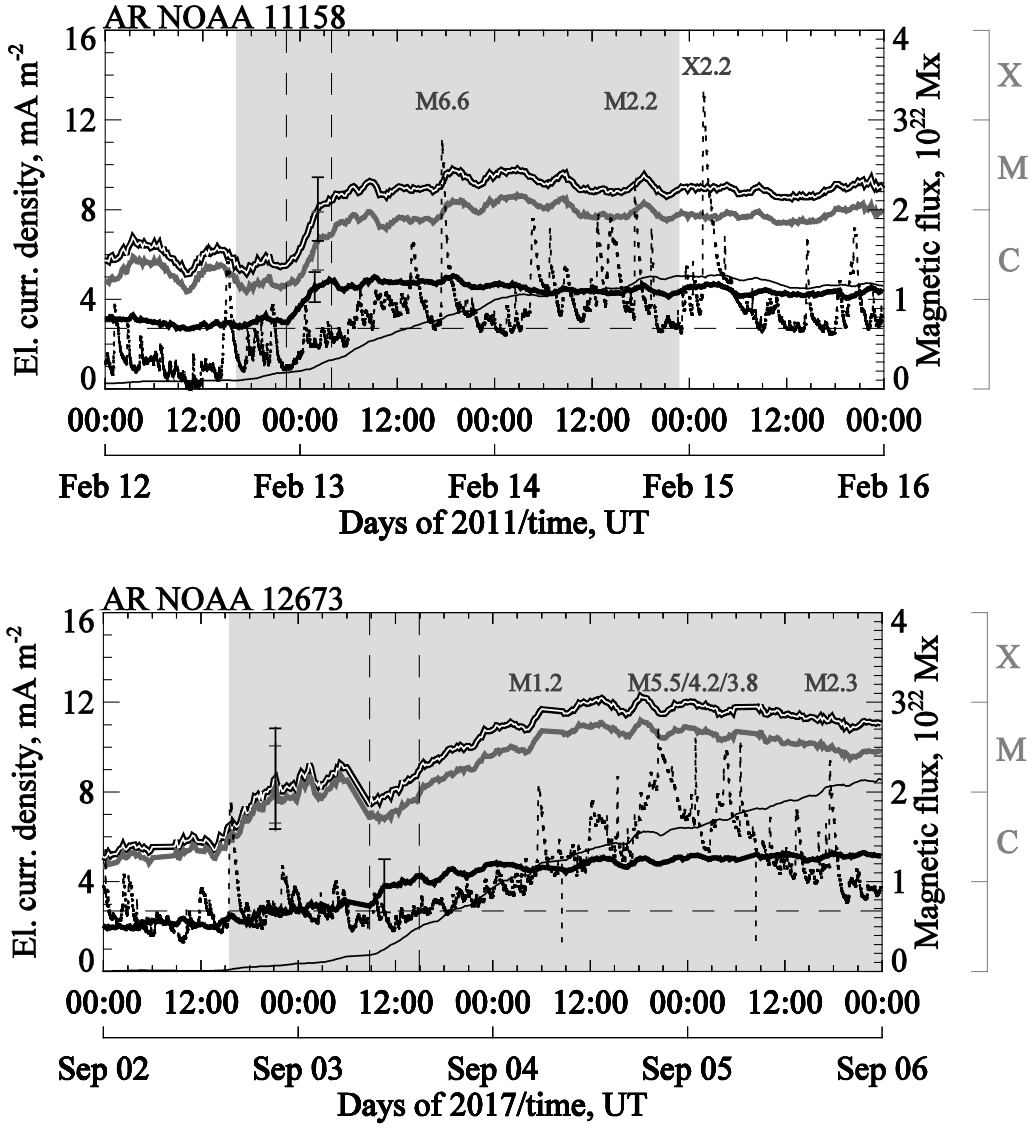
AR NOAA 11158
El. curr. density, mA m-2
Magnetic flux, 10^22 Mx
M6.6
M2.2
X2.2
X
M
C
00:00 12:00 00:00 12:00 00:00 12:00 00:00 12:00 00:00
Feb 12 Feb 13 Feb 14 Feb 15 Feb 16
Days of 2011/time, UT
AR NOAA 12673
El. curr. density, mA m-2
Magnetic flux, 10^22 Mx
M1.2
M5.5/4.2/3.8
M2.3
X
M
C
00:00 12:00 00:00 12:00 00:00 12:00 00:00 12:00 00:00
Sep 02 Sep 03 Sep 04 Sep 05 Sep 06
Days of 2017/time, UT

Fig. 4.

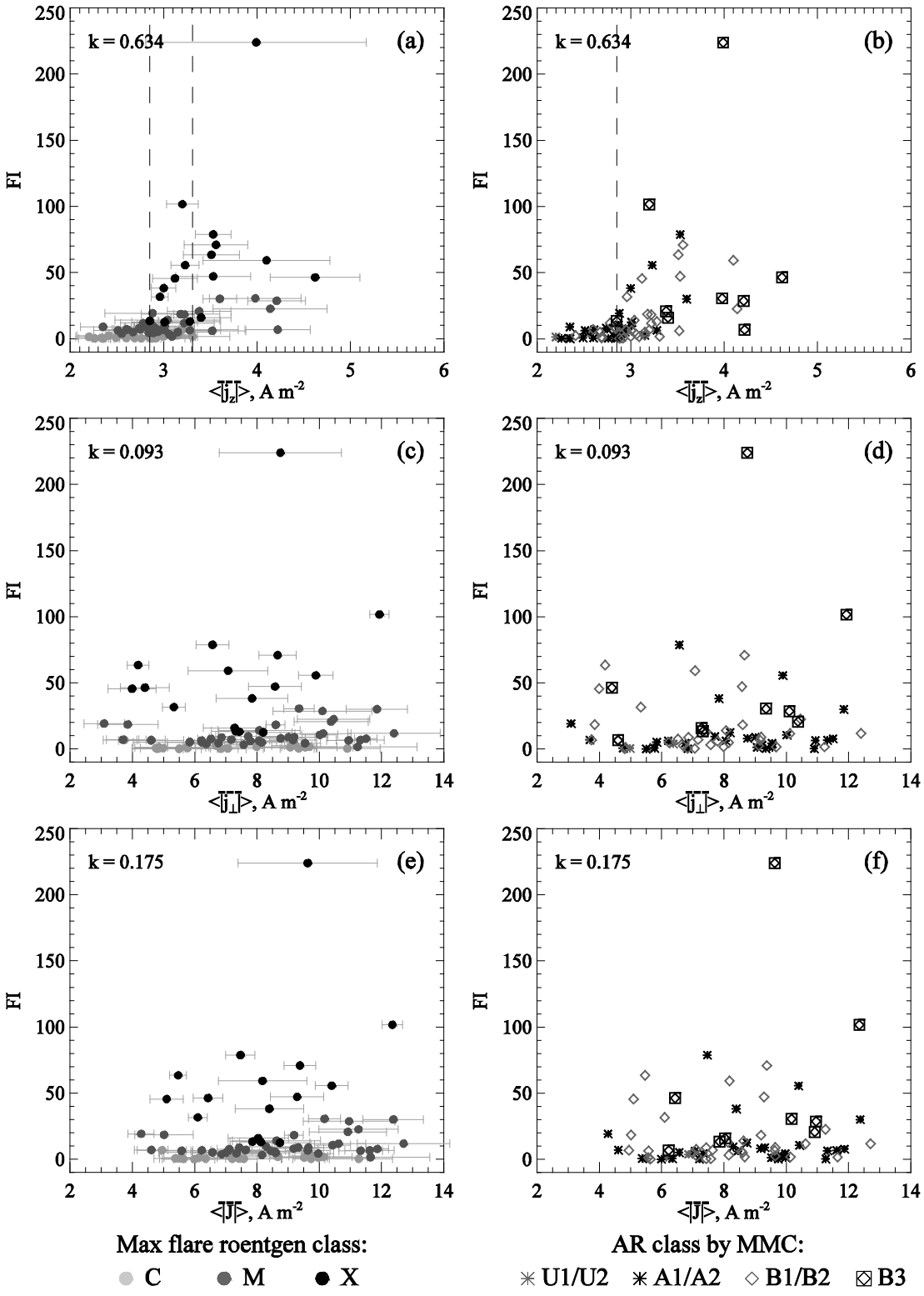
k = 0.634
(a)
k = 0.634
(b)
k = 0.093
(c)
k = 0.093
(d)
k = 0.175
(e)
k = 0.175
(f)
FI
<|j_z|>, A m^-2
<|j_⊥|>, A m^-2
<|J|>, A m^-2
Max flare roentgen class:
C
M
X
AR class by MMC:
U1/U2
A1/A2
B1/B2
B3

Fig. 5.

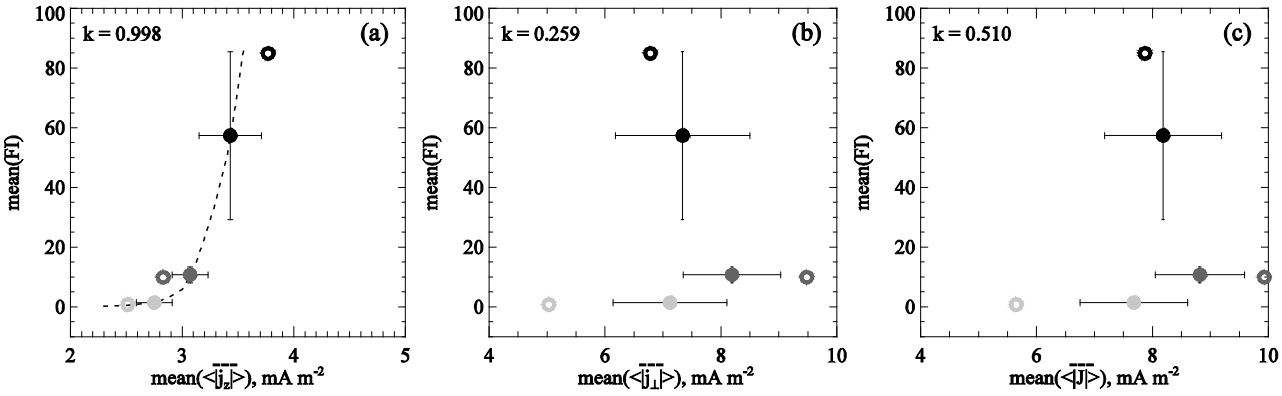
k = 0.998
(a)
k = 0.259
(b)
k = 0.510
(c)
mean(FI)
mean(<|j_z|>), mA m^-2
mean(<|j_⊥|>), mA m^-2
mean(<|J|>), mA m^-2

Fig. 6.